

LARGE EDDY SIMULATION OF A HEAVING WING IN FREESTREAM TURBULENT FLOW

Xiaolu Wang^{1,2}

1. School of Aeronautical Engineering
Zhengzhou University of Aeronautics
450046 Zhengzhou China
Email:wangxl@zua.edu.cn

Zheng-Tong Xie²

2. Faculty of Engineering and Physical Sciences
University of Southampton
SO17 1BJ Southampton UK
Email: z.xie@soton.ac.uk

ABSTRACT

The unsteady aerodynamics of heaving wing in low Reynolds number has received much attention, mainly motivated by the demand of developing micro air vehicles (MAV). Leading edge vortex (LEV) plays a critical role in lift enhancement in the heaving motion. Considering most of MAV operating in turbulent atmosphere boundary, it is necessary to investigate the effects of incoming turbulence on LEV developing and aerodynamic characteristics. Large eddy simulations (LES) of flow over a heaving NACA 0012 wing were conducted to study the effects of inflow turbulence. The reduced frequencies of $k=3.92$ for a chord-normalized amplitude of $h=0.1$ and chord based Reynolds number $Re=10,000$ were used. We found that the turbulent inflow could enhance the thrust for the cases that we investigated. The increase of thrust is 7.3% of the maximum of phase-averaged thrust and 11% of the time-averaged thrust. However, turbulent inflow also leads to 24% increase of R.M.S. of the thrust fluctuations.

1 INTRODUCTION

There is a growing demand for flying drones with diverse capabilities for various applications. Due to smaller size with wingspan between 0.15m-1m (Hassanalian et al., 2017), the Reynolds number of MAV are in the order of $O(10^3) - O(10^4)$ (Baik et al., 2012).

Flapping wing used by insects and small bird species have been inspiring researchers to understand and use the lift enhancement motion in MAV design. It is concluded that the leading edge vortex (LEV) plays a critical role in the lift enhancement under unsteady conditions (Ford et al., 2013). The LEV's main characteristics change as the Reynolds number varies (Shyy et al., 2007). As MAV usually flies in turbulent flow, it is necessary to take incoming turbulence into consideration.

There are intensive analysis on LEV and inflow turbulence effects on unsteady aerodynamics reported in the literature. Experiments on wind turbine blades show that the lift increases along with time delay of the maximum lift in dynamic stall when the turbulence intensity increases (Amandolèse et al., 2004). As for the numerical study, it is showed that the determination of flow separation details are beyond the capability of the RANS

(Reynolds-averaged Navier-Stokes) models. It is suggested that LES or direct numerical simulation (DNS) is a viable alternative (Wang et al., 2017). In an experimental-computational joint study on flow past static SD7003 airfoil, it is shown that the shape and size of the separation bubble are strongly affected by the the incoming turbulence (Schmidt et al., 2017). Studies on wind turbine blade pitching motion show that a turbulence intensity 6% could lead to 50% lift increase during the downstroke, compared to that in smooth inflow (e.g. Kim et al., 2016).

The aerodynamics of heaving wing is relevant and helpful for understanding the flapping mechanism of MAV. It is necessary to analyse LEV developing in incoming turbulent flow. To our knowledge, there is no numerical simulation of inflow turbulence effects on a heaving wing. This paper is focused on this point.

2 NUMERICAL METHODOLOGY

2.1 Governing equations and numerical solver

The governing equations are the filtered unsteady Navier-Stokes equations. For low speed incompressible fluid, the equations are written:

$$\frac{\partial \bar{u}_i}{\partial x_i} = 0, \quad (1)$$

$$\frac{\partial \bar{u}_i}{\partial t} + \frac{\partial \bar{u}_i \bar{u}_j}{\partial x_j} = -\frac{1}{\rho} \frac{\partial \bar{p}}{\partial x_i} + \frac{\partial}{\partial x_j} \left(\nu \frac{\partial \bar{u}_i}{\partial x_j} - \tau_{ij}^r \right), \quad (2)$$

where τ_{ij}^r is the non-linear subgrid-scale(SGS) stress tensor which is modelled:

$$\tau_{ij}^r = \bar{u}_i \bar{u}_j - \bar{u}_i \bar{u}_j, \quad (3)$$

$$\tau_{ij}^r = -2\nu_t \bar{S}_{ij} + \frac{1}{3} \delta_{ij} \tau_{kk}^r, \quad (4)$$

where the Kronecker delta $\delta_{ij} = 1$ for $i = j$, otherwise $\delta_{ij} = 0$; ν_t is the SGS eddy viscosity and \bar{S}_{ij} is the rate-of-strain tensor for the resolved scale:

$$\bar{S}_{ij} = \frac{1}{2} \left(\frac{\partial \bar{u}_i}{\partial x_j} + \frac{\partial \bar{u}_j}{\partial x_i} \right). \quad (5)$$

The mixed-scale (MTS) model (Inagaki et al., 2005) was used. LES computations were carried using OpenFOAM version 2.3.0. A second order implicit scheme was used for the temporal discretization, and the bounded center scheme with a factor $\gamma = 0.25$ is used for the convection term. The pimpleDyMFoam solver was used. Badoe et al. (2019) suggest that the LES model is suitable for heaving wing simulations.

The synthetic divergence-free inflow turbulence generation method (Kim et al., 2013) was used. The inflow velocities can be written as

$$u_i = U_i + a_i u_{*,j}, \quad (6)$$

where $i, j = 1, 2, 3$, u_i is an instantaneous velocity which is imposed at the turbulence inflow location. U_i is a prescribed mean velocity, a_i is a prescribed tensor and $u_{*,j}$ is a velocity fluctuation satisfying the prescribed integral length scales with a zero mean, zero cross-correlations and a unit variance. The details of equation (6) was presented in Kim's paper (Kim et al., 2013).

2.2 Parameters setting and mesh generation

The selected wing is the same as that in the shape is recent experiments and numerical simulations (Chiereghin et al., 2017; Badoe et al., 2019). NACA 0012 airfoil with sharp trailing edge was used and extruded along span direction to generate the wing geometry. The chord of airfoil is 0.0627m and the span of the wing is 0.015675 which is 0.25 chord.

The reduced frequency was defined as $k = \pi fc / U_\infty$, where f is the heaving frequency, c is the chord length of airfoil, U_∞ is the inflow velocity. The heaving motion was modelled with the imposed vertical displacement $y = A \cos(\omega t)$ and the corresponding vertical velocity $v = -A \omega \sin(\omega t)$, where ω is the angular velocity. The peak to peak amplitude of heaving motion h is $0.5c$ (Figure 1), and $\omega = 30$. The Strouhal number is defined as $St = fc / U_\infty$.

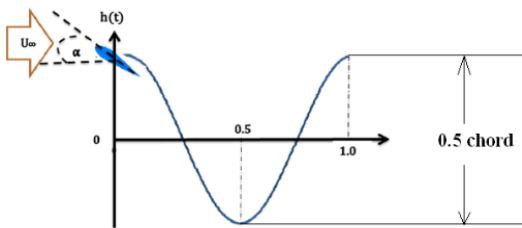
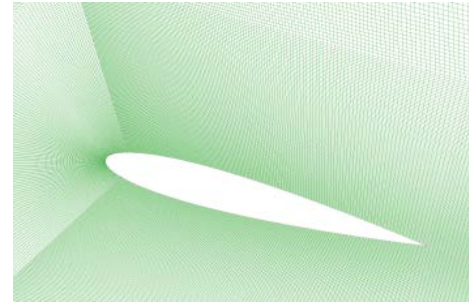
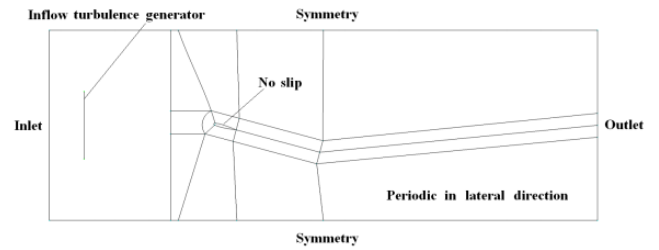


Figure 1. A sketch of heaving motion.

Mesh topology and inflow turbulence generator profile were described in Figure 2. A grid with $645 \times 249 \times 43$ cells was used for the 3D LES computations based on the grid sensitivity analysis (Badoe et al., 2019). For the 2D cases, the domain size and the grid were the same as the cross-section of the 3D case. The inflow turbulence plane was $5.5c$ upstream of the leading edge of the wing for both the 2D and 3D cases. Results show that the maximum y^+ was 8.71, which ensured to resolve the viscous sublayer in the LES computations.



(a) Mesh topology



(b) Domain sketch

Figure 2. Mesh topology and inflow turbulence generation plane location.

2.3 Verification and Validation

Both 2D and 3D LES computations were performed. The inlet velocity was 1m/s and the Reynolds number based on the chord length and the freestream velocity was $Re = 2 \times 10^4$. The reduced frequencies was $k = 0.94$. The angle of attack was $\alpha = 15^\circ$ and the Strouhal number was 0.30.

A comparison for phase-averaged lift coefficients between the 2D, 3D computations and the experimental data are shown in Figure 3. The phased-averaged experimental data and the 2D computational data were obtained through 55 cycles averaging. The number of cycles for the averaging was 3 for the 3D case due to computational cost limit. The 3D results are in a good agreement with former computations (Badoe et al, 2019, not shown here). During upstroke, the 3D results are closer to the experimental data than the 2D results. There are evident oscillations near the maximum lift coefficient for the 3D case, while for the 2D case the oscillation is visible but small. The experimental data don't show such an oscillation at all. Overall the data of 2D LES are reasonable. This confirms that the 2D LES is adequate and effective for studying certain details of the flow field (Martha et al., 2011; Suryanarayanan et al., 2017). The 2D LES is also significantly faster than the 3D LES, and this is crucial for studying such problems.

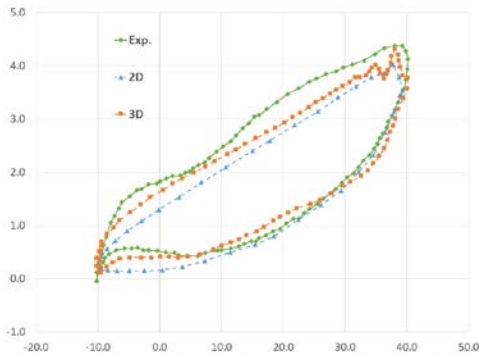


Figure 3. Phase-averaged lift coefficient as a function of effective angle of attack.

3 RESULTS FOR FREESTREAM LAMINAR FLOW

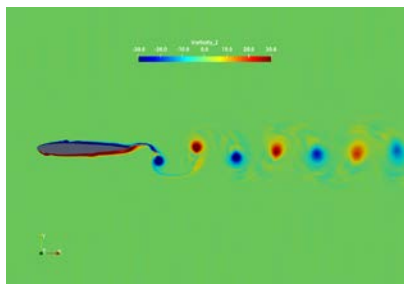
In this section, freestream laminar flow around a heaving airfoil is simulated using the 2D LES. The inlet velocity was 1m/s and the chord based Reynolds number is $Re = 1 \times 10^4$. The reduced frequency is $k=3.92$. The peak to peak amplitude of heaving motion was 0.1 chord. The angle of attack is $\alpha=0^\circ$ and the Strouhal number is 1.25.

Instantaneous vorticity distributions near airfoil are presented in Figure 4. The wake structure (Figure 4a) is consistent with Medjrroubi, et al (2012). New findings based on the development of LEV and Concentrated Vorticity Ejection (CVE) (Doligalski, 1994) are presented below.

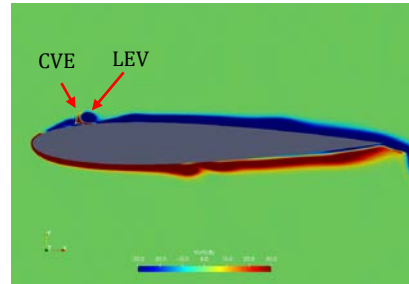
First, the LEVs are generated and convect along the upper and lower surfaces, and merge into the boundary layer (BL) at about three quarters of the chord length.

In the downstroke stage, there is positive vorticity originated behind the LE, with negative vorticity around it. Almost simultaneously as the negative vorticity becomes stronger and forms into an LEV, the positive vorticity underneath the LEV also grows and forms into a CVE. The CVE then isolates the LEV from the upstream flow structures at the leading edge. The initial shape of CVE is a horizontally mirrored λ . Then it changes into a crescent shape, decays and finally disappears. As the CVE decays, the upstream vorticity catches up with the LEV and force the LEV to merge into the BL. The phenomenon of downstroke stage is the to the upstroke one in this configuration.

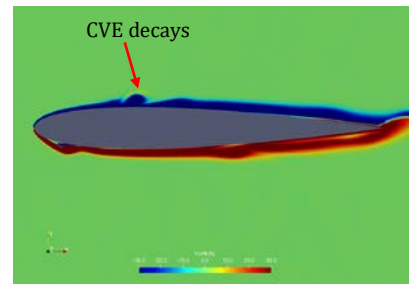
The life time of the CVEs is about one quarter of the heaving period, while the LEV life time is about one half of the heaving period. Considering the upper side for an example, when the LEV decays at about three quarter of the chord length in the downstroke, the lift reaches the minimum value.



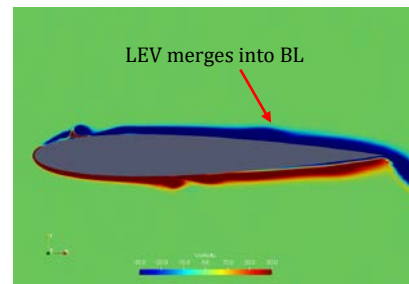
(a) $\phi_t = \frac{29}{100} \cdot T$



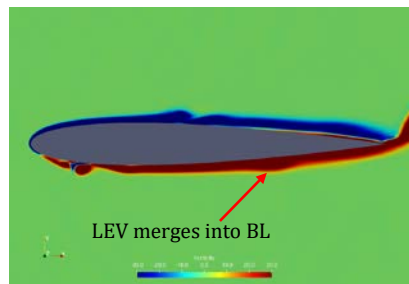
(b) $\phi_t = \frac{1}{100} \cdot T$



(c) $\phi_t = \frac{25}{100} \cdot T$



(d) $\phi_t = \frac{89}{100} \cdot T$



(e) $\phi_t = \frac{146}{100} \cdot T$

Figure 4. Instantaneous vorticity distributions near the airfoil in freestream laminar flow.

4 A HEAVING WING IN FREESTREAM TURBULENT FLOW

4.1 Instantaneous vorticity distribution

In this section, all the settings are the same as those in Section 3 (laminar inflow case) except the implementation of the freestream turbulent inflow (Kim and Xie, 2016). The inflow turbulence is homogeneous and isotropic. The integral length scale is 0.15c, where c is the chord length. The intensity at 1 chord upstream of leading edge is 12% (Figure 5).

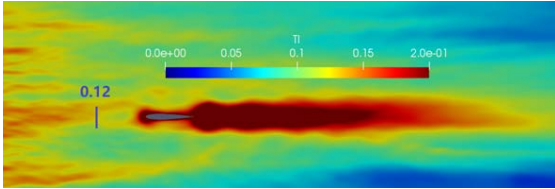
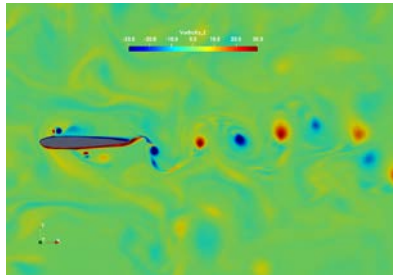


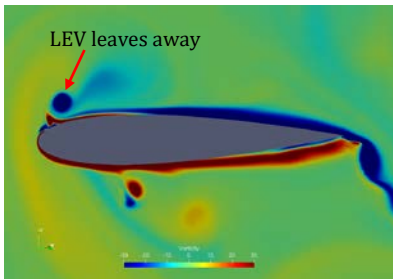
Figure 5. Turbulence intensity distribution around the airfoil.

The instantaneous vorticity distribution at typical time are shown in Figure 6, with the same phase positions in Fig.4. Fig. 6(a) shows that there are complicated interactions between the incoming turbulent eddies and the LEV/CEV/wake vortex. These force the wake vortex bias a greater distance from the central line. The size of the wake vortex also changes evidently.

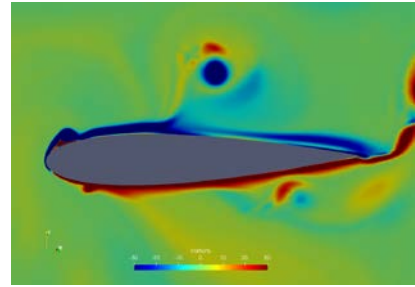
The LEVs convect and merge into the BL (Fig.6(d)) or the wake (Fig.6(e)). It is different from those in laminar inflow, which merge into the BL (Fig. 4(d)). On the upper side, the incoming eddy with positive vorticity ω_z and the CEV induce the LEV to leaves away from the surface (Fig.6(b)), whereas in laminar inflow the LEV always travels close to the surface (Fig.4(b)). On the contrary, the incoming positive eddies suppress the CEV and induce the LEV to move towards the surface on the lower side, (Fig.6(c)-(e)). The CEV decays more slowly if the nearest incoming eddy is in the same direction (Fig.6(b)-(c)).



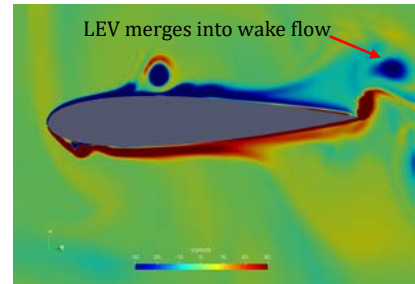
(a) $\phi_t = \frac{29}{100} \cdot T$



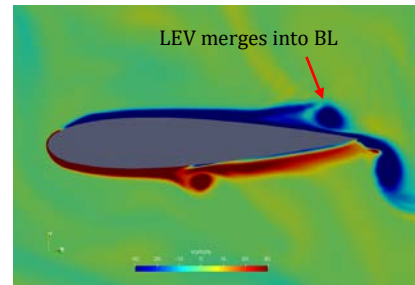
(b) $\phi_t = \frac{1}{100} \cdot T$



(c) $\phi_t = \frac{67}{100} \cdot T$



(d) $\phi_t = \frac{130}{100} \cdot T$



(e) $\phi_t = \frac{200}{100} \cdot T$

Figure 6. Instantaneous vorticity distributions near airfoil for freestream turbulent flow.

4.2 Aerodynamic coefficients

Figure 7 shows the phase-averaged aerodynamic coefficients curves. The freestream turbulent eddies have more significant effect on the drag than lift coefficients (Fig.7). The cap of mushroom could be more tilted to the streamwise direction at certain moments (Fig.6 (a)), leading to extreme thrust (Fig.7 (b)). There are similar trends based on phase-averaged results (Fig.8), the local relative increase of maximum thrust is 7.3%. Based on time-averaged aerodynamic coefficients, the increase is greater. Compared to the laminar inflow, the freestream turbulent flow leads to 11% increase of thrust, and 24% increase of R.M.S. of thrust fluctuations.

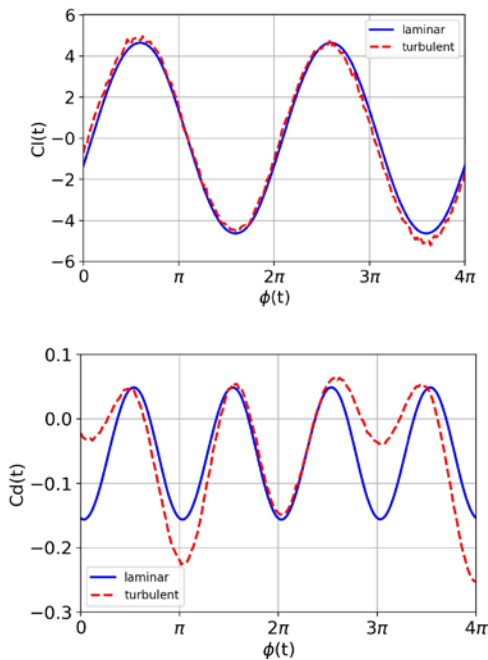


Figure 7. Instantaneous aerodynamic coefficients in 2 heaving cycles for freestream laminar and turbulent flows.

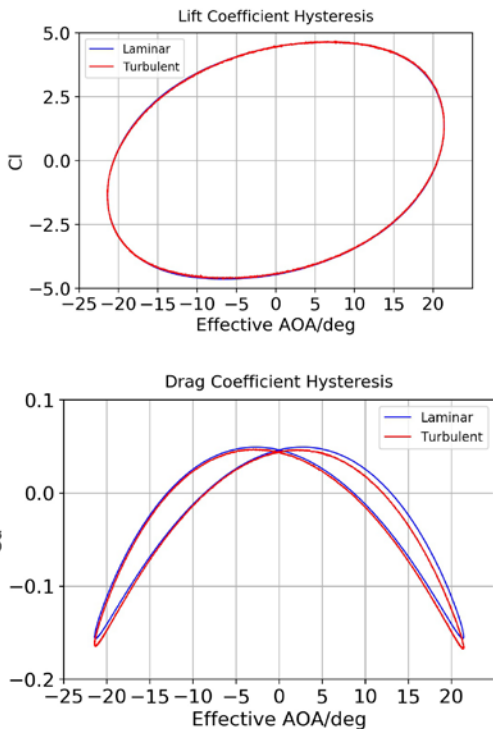


Figure 8. Phase-averaged aerodynamic coefficients in 55 heaving cycles for freestream laminar and turbulent flows.

4.3 Spectrum of velocity and super harmonic frequency

The spectrum of velocity and super harmonic frequency (SHF, or integer multiple of fundamental frequency) are

presented to obtain better insight into the turbulence effects. 11 probes were placed over the upper surface (Fig.9).

For the laminar inflow case, the SHFs on probes 1,3,11 have similar decay trends (Fig.10). For example, the energy at the SHFs decrease at the order of about 1/10 for streamwise velocity component on probe 1, while for vertical velocity the trend is different (Fig.11). On probe 9, the magnitude at $2f_h$ is about 1/100 of u_{th} at f_h .

Fig.11 shows energy spectra of velocity components on probe 1 in laminar and turbulent inflows. Fig.11 shows that inflow turbulence smoothens the variations of the spectrum of the SHFs.

For the turbulent inflow case, the energy spectra also have more evident differences between different probes. Figure 12 shows that 4 SHFs at probe 1 are activated by the LE, 4 SHFs at probe 11 are activated by the TE motion. However, certain SHFs are missing in the areas between those two probes, which is because the LEVs/CEVs decays in the convection.

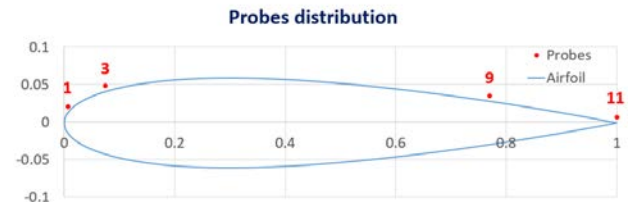


Figure 9. Locations of different probes

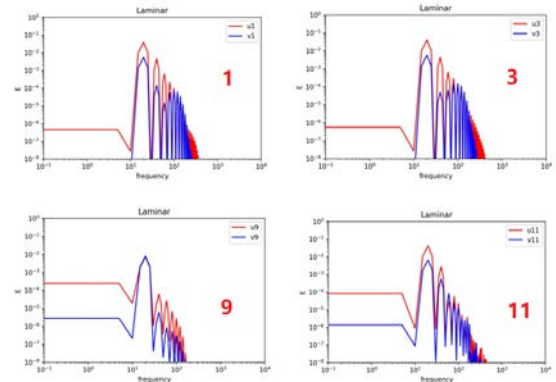
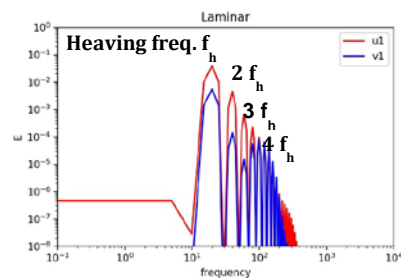
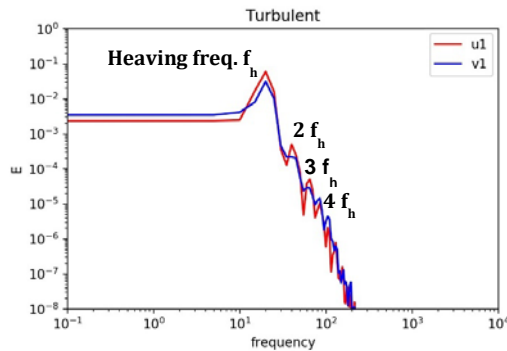


Figure 10. Energy spectra of velocity components on 4 probes for laminar inflow.



(a) Laminar inflow



(b) Turbulent flow

Figure 11. Energy spectra of velocity components on probe 1 for laminar and turbulent inflows.

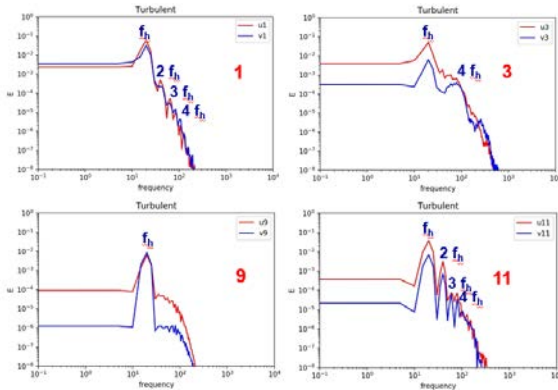


Figure 12. Energy spectra of velocity components on 4 probes for turbulent inflow.

5. CONCLUDINGS

We investigated the effects of turbulent inflow on aerodynamic characteristics of a heaving wing using 2D large eddy simulations (LES). The comparison for phase-averaged lift coefficients between 2D, 3D computations and experimental data show that the 2D LES approach is reasonable and acceptable. We found that on the upper side, the incoming positive eddy and positive CEV induces negative LEV to leave away from the surface. On the lower side, the incoming positive eddy suppresses the negative CEV and induces the positive LEV to move towards the surface. Freestream turbulence leads to a significant increase of the R.M.S. of the thrust fluctuation, compared to the laminar inflow. Future work should focus on the investigation of the effects of turbulent intensity, integral length scale and angle of attack.

ACKNOWLEDGEMENT

The authors acknowledge the use of IRIDIS4 High Performance Computing Facility at the University of Southampton. The financial support of XW by the China Scholarship Council is gratefully acknowledged. XW also acknowledge the hospitality provided by the Engineering

Faculty of the University of Southampton during his one year visit.

REFERENCES

Amandolèse X., Széchenyi E., 2004, "Experimental Study of the Effect of Turbulence on a Section Motionl Blade Oscillating in Stall", *Wind Energy*, Vol. **7**, pp. 267-282.

Badoe C. E., Xie Z.T., Sandham N. D., 2019, "Large Eddy Simulation of a Heaving Wing on the Cusp of Transition to Turbulence", *Computers and Fluids*, Vol. **184**, pp. 64-77.

Baik Y. S., Bernal L. P., Granlund K, et al., 2012, "Unsteady force generation and vortex dynamics of pitching and plunging aerofoils", *Journal of Fluid Mechanics*, Vol. **709**, pp. 37-68.

Doligalski T. L., Smith C. R., Walker J. D. A., 1994, "Vortex interactions with walls", *Annual Review of Fluid Mechanics*, Vol. **26**, pp. 573-616

Ford C.W.P., Babinsky H., 2013, "Lift and the Leading Edge Vortex", *Journal of Fluid Mechanics*, Vol. **720**, pp. 280-313.

Hassanalian M., Abdelkefi A., 2017, "Classifications, applications, and design challenges of drones: A review", *Progress in Aerospace Sciences*, Vol. **91**, pp. 99-131.

Inagaki M., Kondoh T., Nagano Y., 2005, "A mixed-time-scale SGS model with fixed model-parameters for practical LES". *Journal of Fluids Engineering*. Vol. **127**, pp.1-13.

Kim Y., Xie Z-T., 2016, "Modelling the effect of freestream turbulence on dynamic stall of wind turbine blades", *Computers and Fluids*, Vol. **129**, pp. 53-66.

Martha C. S., Blaisdell G A, Lyrintzis A. S., 2011, "Large eddy simulations of 2-D and 3-D spatially developing mixing layers". AIAA 2011-830.

Medjroubi W., Stoevesandt B., Peinke J., 2012, "Wake classification of heaving airfoils using the spectral/hp element method. *Journal of Computational and Applied Mathematics*, Vol. **236**:pp.3774-3782.

Schmidt S., Breuer M., 2017, "Source term based synthetic turbulence inflow generator for eddy-resolving predictions of an airfoil flow including a laminar separation bubble", *Computers and Fluids*, Vol. **146**, pp. 1-22.

Shyy W., Liu H., 2007, "Flapping Wings and Aerodynamic Lift: The Role of Leading-Edge Vortices", *AIAA Journal*, Vol. **45**, pp. 2817-2819.

Suryanarayanan S., Narasimha R., 2017, "Insights into the growth rate of spatially evolving plane turbulent free-shear layers from 2D vortex-gas simulations". *Physics of Fluids*, Vol. **29**: 020708

Wang L., Fu S., 2017, "Detached-eddy simulation of flow past a pitching NACA 0015 airfoil with pulsed actuation", *Aerospace Science and Technology*, Vol. **69**, pp 123-135.